

# Localization of Exudate for Diabetic Retinopathy using Convolutional Neural Networks

Janhvi Chauhan<sup>1</sup>, Dhaval Modi<sup>2</sup>

<sup>1,2</sup>Lecturer

<sup>1,2</sup>Electronics & Communication Dept., Government Polytechnic, Ahmedabad

## Abstract

In order to track the progression of diabetic retinopathy (DR), exudate detection is a crucial task for computer-aided diagnosis of DR. This article uses a deep convolutional neural network (CNN) to identify exudates at the pixel level. The CNN model is saved as an offline classifier once it has been trained using expert-labelled exudate picture patches. Potential exudate candidate sites are first retrieved using the morphological ultimate opening approach in order to obtain pixel-level accuracy while cutting down on computing time. The trained CNN model is then used to classify and identify the local region ( $64 \times 64$ ) around the candidate points. The suggested CNN architecture achieves a pixel-wise accuracy of 89.50%, sensitivity of 87.00%, and specificity of 94.23% on the test database.

**Keywords:** Diabetic Retinopathy, Optic Disc, exudates, Retinal Vessels

## 1. Introduction

In developed nations, diabetic retinopathy (DR) is the primary cause of blindness and visual loss in people of working age [1], [2]. For diabetics, early identification and annual screening are essential to preventing more visual loss [1]. Automatic DR grading has the potential to reduce the burden of ophthalmologists, increase efficiency, and lower the cost of DR screening, especially in light of the constantly growing number of diabetes patients [3]–[5]. When the blood-retinal barrier breaks down, serum proteins, lipids, and proteins can escape from the capillaries, resulting in exudate [2]. It is among the early clinical indicators of DR. Consequently, the diagnosis of DR depends on the precise and automated identification of exudate. In colour fundus imaging, exudates appear as brilliant white or yellow objects with varying contrast and forms. Figure: 1 displays a typical DR image with exudate.



**Figure: 1 DR color fundus image with exudates presented**

Numerous methods have been developed for the broad investigation of automatic exudate detection. Exudate detection is usually broken down into three main steps: obtaining exudate candidates, feature extraction, and machine learning. For the purpose of extracting the exudate candidates, a number of

techniques have been developed. These include morphological operation-based methods, such as [6], [7], clustering-based methods, such as [8], [9], and pixel-level feature-based machine learning, such as [10], [11]. Following the acquisition of exudate candidates, the candidate points are often further classified using feature extraction and machine learning. For all of the exudate candidates, Zhang et al. retrieved 28 features, including those related to intensity, geometry, and texture. Random forest was then used for classification [6]. For the exudate candidates, Garcia et al. collected 18 features, including color and form features, and tried various machine learning techniques, such as support vector machines, radial basis functions, and multilayer perceptron, for classification [23].

In this work, we integrated deep neural networks with image processing procedures to increase the pixel-level exudate detection accuracy. The ultimate opening algorithm is used to obtain viable candidates. After that, the immediate area around the seed points is taken out and sent to deep convolutional neural networks that have been trained for classification. Consequently, accurate exudate detection at the pixel level is achieved.

## 2. Method and Methodology

Figure 2 shows the general framework for the detection of exudates. The  $64 \times 64$  patches taken from the illumination-corrected green channel image are used to train the CNN network, and the trained model is then saved on the computer. The optic disc and blood vessels are first eliminated from the retinal pictures as part of the image processing process. The prospective exudate candidates, or seed points, are then obtained using the ultimate opening algorithm. Finally, the trained deep learning model is fed the local patches surrounding the seed sites to determine whether or not they are exudates.

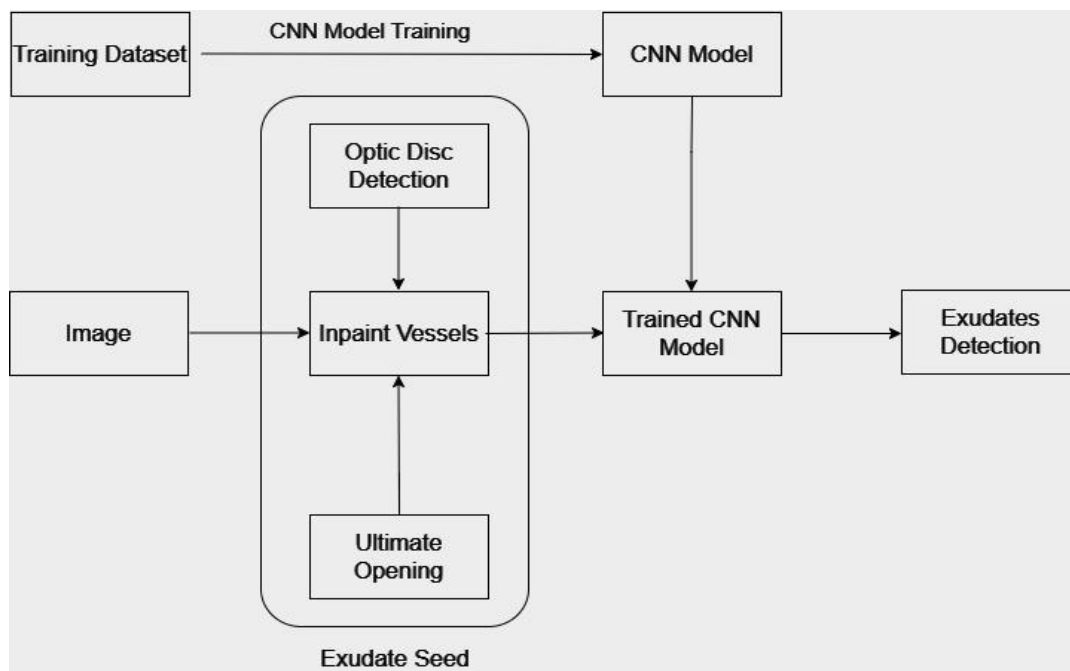


**Figure 2 Framework for exudate detection with deep learning**

If all of the pixels inside the fundus image are calculated, it would take a lot of time to apply the CNN model to each pixel in order to accomplish pixel-level identification for a pure deep learning approach. Thus, the benefit of employing the ultimate opening method is that it will efficiently identify the possible target candidate and eliminate the background points. The process will proceed more quickly if the ultimate opening reduces the candidate numbers to 1-20% of the entire pixel number in the image, depending on the symptoms of the exudate in the fundus image.

### A. Removal of Optic Disc Detection

Since exudates and the optic disc are both bright objects with comparable colors in a color fundus image, the optic disc must be identified and masked out before the exudates can be recognized effectively. The local phase symmetry technique is used to detect optic discs. A dimensionless indicator of the level of feature symmetry in the immediate area is the local phase symmetry algorithm [13]. The middle of the optic disc responds strongly because it shows on the retinal image as a brilliant circular or elliptic zone. The whole optic disc region is then extracted from the highest response of local phase symmetry via region growth. The optic disc radius is the smallest circle radius that surrounds the area that is growing.

### B. Removal of Retinal Vessels

Retinal vessels are typically removed by segmenting the vessel and then inpainting it in accordance with the segmentation outcome. The fine vessels are difficult to segment and remove, which is a drawback of this popular technique. Zhang et al. suggested inpainting the dark structures (vessels, microaneurysms, hemorrhages, etc.) by using morphological closure and opening operations, followed by the supremum operation [7]. We used this method in our study because it effectively removed tiny black lesions and fine arteries while leaving the light lesions intact. The inpainting outcome for the green channel retinal imaging displayed in Figure: 3(a) is displayed in Figure: 3(b).

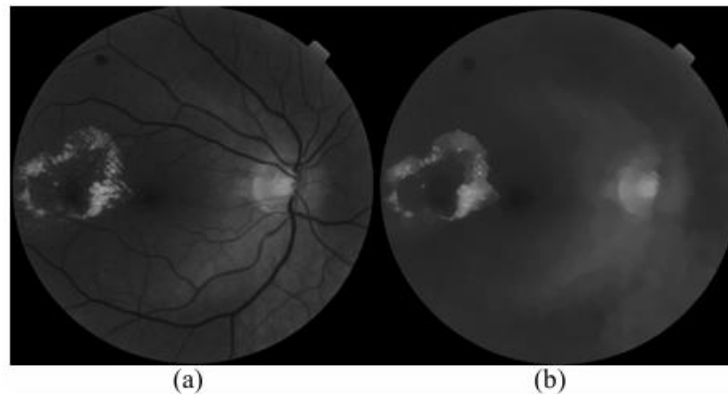


**Figure: 3 Removal of tiny black lesions and retinal vessels. (A) The fundus image in green channel color; (B) the vessel and little dark lesion eliminated outcome image (b).**

### C. Ultimate Opening

The final opening is used to obtain the exudates candidate points following the removal of the retinal vasculature and small black lesions. Beucher was the first to propose ultimate opening, a residual operator that emphasizes the most contrasted patterns [14], [15]. The maximum residue is chosen as the temporary outcome after the image is subjected to a series of opening operations with progressively larger structure elements. Until the maximum specified structural element size is attained, this phase is repeated. Figure: 4(a) displays the final opening result of the image Figure: 3(a). The appropriate threshold inside a specific structuring element encircling the local region is determined using the region-based Otsu algorithm; the outcome is displayed in Figure: 4(b).

However, the binary image in Figure: 4(b) does not accurately depict all of the possible exudate candidate locations when compared to the original image in Figure: 3(a). While some areas are larger than the actual exudates, others are smaller. We then inpaint the slightly dilated binary picture (Figure: 4(b)) on the original green channel image to refine the possible candidate result. The difference between the inpainted and original images is then obtained, as illustrated in Figure: 4(c). After that, the difference image is segmented to produce a more precise exudate candidate image, as seen in Figure: 4(d).

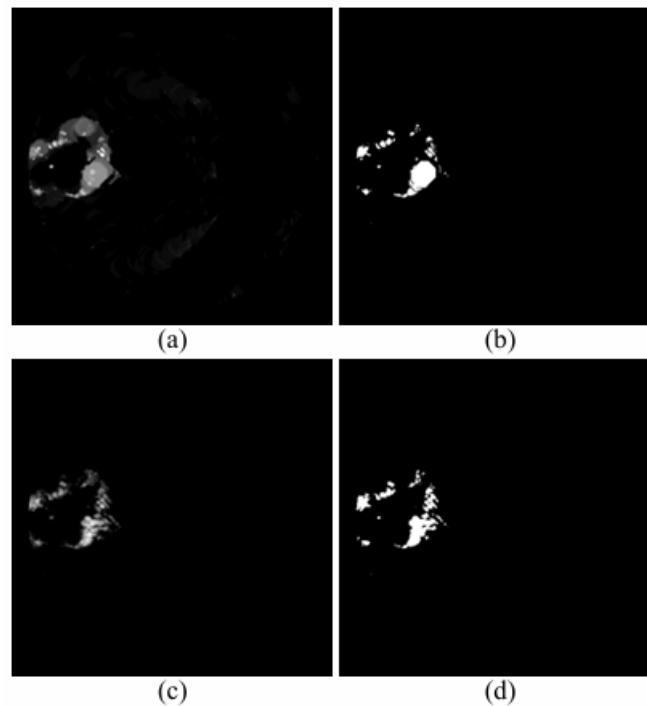


**Figure: 4** Use the ultimate opening algorithm to get exudate candidate points. (b) segment ultimate opening result with local Otsu thresholding; (a) ultimate opening result; (d) the image of possible exudate candidates; (c) the difference image, which is produced by subtracting the inpainted image from the green channel image;

#### D. Convolutional Neural Networks

CNN differs from other conventional machine learning techniques in that it uses training images to automatically learn features rather than expertly created features like support vector machines and random forests do. Its efficacy in picture recognition and classification has been demonstrated [17], [18]. Convolutional, pooling, and fully-connected layers are the three primary types of layers that typically make up a CNN architecture. A complete CNN architecture is created by stacking the three different kinds of layers.

The size and quantity of the learnable filters in the convolutional layer can be adjusted by the user, while the weights are automatically determined and refined throughout the training process. In general, the deeper convolutional layers can learn more abstract, or high-level, features, whereas the initial layers will learn simpler features, such as edges. All of the convolution responses between the input channels with the filters are added together, and an element-wise non-linear activation function—a rectified linear unit in this study—is then applied to the total to determine the convolutional layer's output.

To gradually reduce the spatial dimension and further minimize the network's computation time, a pooling layer—typically a max-pooling layer—must be added in between each convolutional layer. The convolutional layer's most notable response in the local area will be chosen via max-pooling. The stride, or downsample ratio, is one of the tunable parameters in the max-pooling parameter; typically, 2 is employed.

Following a few stacks of max-pooling and convolutional layers, high-level abstract features with the appropriate dimensions are retrieved. For final classification, the output from the final max-pooling layer is subsequently sent to the fully linked layer. Essentially, a fully connected layer is a conventional multi-layer perceptron with an output layer that employs a softmax activation function. Using the high-level characteristics produced by earlier layers, the fully connected layer's goal is to categorize the input image into different groups according to the training dataset. A dropout layer is included between the fully-

connected layers to regularize the network and prevent over-fitting. During training, the dropout layer will randomly remove neurons and their connections, preventing neurons from over-co-adapting.

No.	Layer Type	Maps	Size	KerSize
0	Input Layer	1	64 × 64	---
1	Convolutional	32	62 × 62	3 × 3
2	Convolutional	32	60 × 60	3 × 3
3	MaxPool	32	30 × 30	2 × 2
4	Convolutional	64	28 × 28	3 × 3
5	Convolutional	64	26 × 26	3 × 3
6	MaxPool	64	13 × 13	2 × 2
7	Convolutional	96	11 × 11	3 × 3
8	Convolutional	96	9 × 9	3 × 3
9	MaxPool	96	4 × 4	2 × 2
10	Convolutional	128	2 × 2	3 × 3
11	MaxPool	128	1 × 1	2 × 2
12	Fully-Connected	64 Neurons		
13	DropOut	64 Neurons		
14	Fully-Connected	64 Neurons		
	Output Layer	2 Neurons		

**Table 1 CNN Architecture**

Table I provides the CNN network architecture. 64×64 patches taken from the illumination-corrected green channel image are fed into the network. The CNN model is trained independently using illumination-corrected green channel images and expert annotations. The CNN training method uses only a few image processing algorithms, with the exception of lighting correction, which eliminates brightness variance. The CNN model will be stored as a classifier for subsequent use once it has been appropriately trained.

### 3. Result

E-Ophtha EX, a recently released open-source database for exudate segmentation with pixel-level annotations by two experts [7], was the database used in this study. The total number of photographs in E-Ophtha Ex is 82, comprising 35 normal photos and 47 exudate images. Every photograph, which ranges in size from 1440 960 pixels to 2544 1696 pixels, was taken with a field of view of 45. The image sizes in this study are normalized to have a disc radius of 70 pixels, which yields an image dimension of about 1200 800, in order to standardize the processing settings.

We retrieved all of the positive expert-labeled annotations from the 32 randomly chosen training photos—roughly 70% of the 47 exudate images in the database—for the CNN network's training. A random selection of 30% of the training data is set aside for the performance test. The pixels with no exudates are chosen at random to form the negative patches. The number of negative examples chosen is equal to the number of positive samples in order to maintain the balance between the two classes. A total of 249,448 patches—122,036 positive patches and 127,412 negative patches—are used to train and validate the CNN network. A total of 114,922 patches from 15 exudate photos make up the test set, which includes 65,510 positive patches and 49,412 negative patches. We train the CNN model using the Theano, Lasagne, and Nolearn deep learning libraries. 150 epochs have been used to train the network.

	Training Set (%)	Test Set (%)
Accuracy	95.3%	89.50%
Sensitivity	93.08%	87.00%
Specificity	96.32%	94.23%
F-Score	95.36%	91.38%

**Table 2 performance of the proposed CNN architecture.**

The performance of the suggested CNN architecture on training and test databases is shown in Table II. On the test set, an accuracy of 89.50% is attained. In contrast, Zhang et al. used the random forest method on the same dataset at the pixel level and obtained a sensitivity of 74% and a positive predictive value of 72%. Even if the contrast and image quality may differ, the accuracy on the test set shows that the trained CNN model has strong generalization ability given that the training and test datasets are randomly split at the image level.

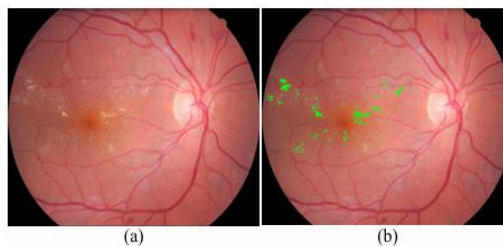


**Figure: 5 Exudate identification using the suggested method. (a), the original image with exudate; (b), exudate identified by the algorithm is marked in green.**

For the image on Figure: 5(a), Figure: 5(b) provides an example of the identification result using the suggested approach. It can detect the exudate down to the pixel level.

#### 4. Conclusion

In this work, we suggested a deep learning-based approach for pixel-level exudate identification. After using morphological ultimate opening approaches to extract a collection of exudate candidates, the candidate points are sent to CNN deep networks that have been trained for classification. For both the test and training sets, the method's pixel-by-pixel accuracy was high.

Testing the approach on more publicly accessible databases, such as the IRDRand DIARETDB databases, will be part of future study. Furthermore, because of the nature of deep learning and machine learning, increasing the quantity and variety of training data will typically result in better model performance. More exudate photos, like the manual labelling offered by DIARETDB1, could be included to the training set in the future.

#### References

1. M. D. Abr'amoff, M. K. Garvin, and M. Sonka, "Retinal imaging and image analysis," IEEE Reviews in Biomedical Engineering, vol. 3, pp. 169–208, 2010.
2. T. A. Ciulla, A. G. Amador, and B. Zinman, "Diabetic retinopathy and diabetic macular edema: Pathophysiology, screening, and novel therapies," Diabetes Care, vol. 26, no. 9, pp. 2653–2664, 2003.

3. A. Sopharak, B. Uyyanonvara, S. Barman, and T. H. Williamson, "Automatic detection of diabetic retinopathy exudates from non-dilated retinal images using mathematical morphology methods," *Computerized Medical Imaging and Graphics*, vol. 32, no. 8, pp. 720–727, 2008.
4. T. Teng, M. Lefley, and D. Claremont, "Progress towards automated diabetic ocular screening: a review of image analysis and intelligent systems for diabetic retinopathy.," *Medical & biological engineering & computing*, vol. 40, no. 1, pp. 2–13, 2002.
5. N. Patton, T. M. Aslam, T. MacGillivray, I. J. Deary, B. Dhillon, R. H. Eikelboom, K. Yogesan, and I. J. Constable, "Retinal image analysis: Concepts, applications and potential," *Progress in Retinal and Eye Research*, vol. 25, no. 1, pp. 99–127, 2006.
6. A. Osareh, M. Mirmehdi, B. Thomas, and R. Markham, "Automated identification of diabetic retinal exudates in digital colour images.," *The British journal of ophthalmology*, vol. 87, no. 10, pp. 1220–3, 2003.
7. X. Zhang, G. Thibault, E. Decenci`ere, B. Marcotegui, B. La`y, R. Danno, G. Cazuguel, G. Quelled, M. Lamard, P. Massin, A. Chabouis, Z. Victor, and A. Erginay, "Exudate detection in color retinal images for mass screening of diabetic retinopathy," *Medical Image Analysis*, vol. 18, no. 7, pp. 1026–1043, 2014.
8. Feroui Amel and Messadi Mohammed and Bessaid Abdelhafid, "Improvement of the Hard Exudates Detection Method Used For Computer- Aided Diagnosis of Diabetic Retinopathy," *I.J. Image, Graphics and Signal Processing*, no. May, pp. 19–27, 2012.
9. M. Niemeijer, B. Van Ginneken, S. R. Russell, M. S. A. Suttorp-Schulten, and M. D. Abr`amoff, "Automated detection and differentiation of drusen, exudates, and cotton-wool spots in digital color fundus photographs for diabetic retinopathy diagnosis," *Investigative Ophthalmology and Visual Science*, vol. 48, no. 5, pp. 2260–2267, 2007.
10. M. Garcia, C. I. S´anchez, M. I. L´opez, D. Ab´asolo, and R. Hornero, "Neural networkbased detection of hard exudates in retinal images," *Computer Methods and Programs in Biomedicine*, vol. 93, no. 1, pp. 9–19, 2009.
11. A. Sopharak, K. T. Nwe, Y. A. Moe, M. N. Dailey, and B. Uyyanonvara, "Automatic Exudate Detection with a Naive Bayes Classifier," *Proceedings of the International Conference on Embedded Systems and Intelligent Technology*, vol. 1, pp. 139–142, 2008.
12. B. Singh and K. Jayasree, "Implementation of diabetic retinopathy detection system for enhance digital fundus images," *International Journal of advanced technology and innovation research*, vol. 7, no. 6, pp. 874–876,
13. J. Fabrizio and B. Marcotegui, "Fast implementation of the ultimate opening," *Lecture Notes in Computer Science (including subseries Lecture Notes in Artificial Intelligence and Lecture Notes in Bioinformatics)*, vol. 5720 LNCS, pp. 272–281, 2009.
14. T. Walter, J.-C. Klein, P. Massin, and A. Erginay, "A contribution of image processing to the diagnosis of diabetic retinopathy–detection of exudates in color fundus images of the human retina.," *IEEE transactions on medical imaging*, vol. 21, no. 10, pp. 1236–1243, 2002.
15. S. Beucher, "Numerical residues," *Image and Vision Computing*, vol. 25, no. 4 SPEC. ISS., pp. 405–415, 2007.
16. A. Krizhevsky, I. Sutskever, and G. E. Hinton, "ImageNet Classification with Deep Convolutional Neural Networks," *Advances in Neural Information Processing Systems*, pp. 1–9, 2012.
17. K. Simonyan and A. Zisserman, "Very Deep Convolutional Networks for Large-Scale Image Recognition," *International Conference on Learning Representations*, pp. 1–14, 2015.
18. D. J. Browning, *Diabetic retinopathy: evidence-based management*. Springer Science & Business Media, 2010.

19. Nayak, J., Bhat, P. S., Acharya, U. R., Lim, C. M., and Kagathi, M., Automated identification of different stages
20. E. M. Shahin, T. E. Taha, W. Al-Nuaimy, S. El Rabaie, O. F. Zahran, and F. E. A. El-Samie, "Automated detection of diabetic retinopathy in blurred digital fundus images," in Computer Engineering Conference (ICENCO), 2012 8th International. IEEE, 2012, pp. 20-25.
21. M. Shamsujjoha, and T. Bhuiyan, "A Content-based Image Retrieval Semantic Model for Shaped and Unshaped Objects", Journal of Computer Engineering, vol: 18, no: 1, pp:43-60, year: 2016
22. B. Singh and K. Jayasree, "Implementation of diabetic retinopathy detection system for enhance digital fundus images," International Journal of advanced technology and innovation research, vol. 7, no. 6, pp. 874–876
23. P. Kovesi, "Symmetry and asymmetry from local phase," Tenth Australian Joint Conference on Artificial Intelligence, pp. 2–4, 1997.